



HAL
open science

Otogelin, otogelin-like, and stereocilin form links connecting outer hair cell stereocilia to each other and the tectorial membrane

Paul Avan, Sébastien Le Gal, Vincent Michel, Typhaine Dupont, Jean-Pierre Hardelin, Christine Petit, Elisabeth Verpy

► To cite this version:

Paul Avan, Sébastien Le Gal, Vincent Michel, Typhaine Dupont, Jean-Pierre Hardelin, et al.. Otogelin, otogelin-like, and stereocilin form links connecting outer hair cell stereocilia to each other and the tectorial membrane. *Proceedings of the National Academy of Sciences of the United States of America*, 2019, 116 (51), pp.25948-25957. 10.1073/pnas.1902781116 . pasteur-02860028

HAL Id: pasteur-02860028

<https://pasteur.hal.science/pasteur-02860028>

Submitted on 8 Jun 2020

HAL is a multi-disciplinary open access archive for the deposit and dissemination of scientific research documents, whether they are published or not. The documents may come from teaching and research institutions in France or abroad, or from public or private research centers.

L'archive ouverte pluridisciplinaire **HAL**, est destinée au dépôt et à la diffusion de documents scientifiques de niveau recherche, publiés ou non, émanant des établissements d'enseignement et de recherche français ou étrangers, des laboratoires publics ou privés.

Full title

Otogelin, otogelin-like, and stereocilin form links connecting outer hair cell stereocilia to each other and the tectorial membrane

Paul Avan^{a,b}, Sébastien Le Gal^c, Vincent Michel^c, Typhaine Dupont^c, Jean-Pierre Hardelin^c, Christine Petit^{b,c,d,1,2}, and Elisabeth Verpy^{c,1,2}

¹C.P. and E.V. contributed equally to this work

²To whom correspondence should be addressed. Email: christine.petit@pasteur.fr or elisabeth.verpy@pasteur.fr

^aLaboratoire de Biophysique Sensorielle, Université Clermont Auvergne, Inserm UMR 1107, Centre Jean Perrin, Clermont-Ferrand

^bInstitut de l'Audition, Paris, France

^cUnité de Génétique et Physiologie de l'Audition, Institut Pasteur, Inserm UMRS 1120, Paris, France

^dCollège de France, Paris, France

Competing interest statement: Christine Petit and Guy P. Richardson are co-authors on a 2019 review article and co-edited the volume in which it appears.

Short running title

Hair-bundle links in cochlear outer hair cells

Keywords: outer hair cells, hair-bundle links, horizontal top connectors, tectorial membrane-attachment crowns, otoacoustic emissions

Abstract

The function of outer hair cells, the mechanical actuators of the cochlea, involves the anchoring of their tallest stereocilia in the tectorial membrane, an acellular structure overlying the sensory epithelium. Otogelin and otogelin-like are tectorial membrane proteins related to secreted epithelial mucins. Defects in either cause the DFNB18B and DFNB84B genetic forms of deafness, respectively, both characterized by congenital mild-to-moderate hearing impairment. We show here that mutant mice lacking otogelin or otogelin-like have a marked outer hair cell dysfunction, with almost no acoustic distortion products despite the persistence of some mechano-electrical transduction. In both mutants, these cells lack the horizontal top connectors, which are fibrous links joining adjacent stereocilia, and the tectorial membrane-attachment crowns coupling the tallest stereocilia to the tectorial membrane. These defects are consistent with the previously unrecognized presence of otogelin and otogelin-like in the outer hair cell hair bundle. The defective hair bundle cohesiveness and the absence of stereociliary imprints in the tectorial membrane observed in these mice have also been observed in mutant mice lacking stereocilin, a model of the DFNB16 genetic form of deafness, also characterized by congenital mild-to-moderate hearing impairment. We show that the localizations of stereocilin, otogelin, and otogelin-like in the hair bundle are interdependent, indicating that these proteins interact to form the horizontal top connectors and the tectorial membrane-attachment crowns. We therefore suggest that these two outer hair cell-specific structures have shared mechanical properties mediating reaction forces to sound-induced shearing motion and contributing to the coordinated displacement of stereocilia.

Significance statement

Patients lacking either otogelin or otogelin-like present congenital, mild-to-moderate hearing impairment similar to that in patients lacking stereocilin. Stereocilin is associated with two types of links specific to the mechanosensitive antenna (hair-bundle stereocilia) of cochlear outer hair cells: the horizontal top connectors joining stereocilia to each other and the attachment crowns coupling the tallest stereocilia to the tectorial membrane, an acellular structure overlying the sensory epithelium of the cochlea. By studying mutant mice lacking otogelin or otogelin-like, and analyzing the distribution of these proteins, we show that they interact, directly or indirectly, with stereocilin to form the horizontal top connectors and tectorial membrane-attachment crowns, two structures likely satisfying similar mechanical requirements for cooperative stereociliary motion indispensable for optimal cochlear performance.

The sensory epithelium of the cochlea, the organ of Corti, is covered by an acellular structure, the tectorial membrane (TM), and contains two types of sensory cells: the inner hair cells (IHCs), organized into a single row, and the outer hair cells (OHCs), organized into three rows along the longitudinal axis of the cochlea (tonotopic axis). IHCs transmit acoustic information to the primary auditory neurons, whereas OHCs are mechanical actuators: the periodic contraction and elongation of their cell bodies (somatic electromotility), driven by oscillations of their membrane potential, locally amplifies the sound-induced vibrations of the cochlear partition, endowing the auditory organ with its great sensitivity and site-selective responsiveness to the different frequency components of sound waves. Sound-induced vibrations of the organ of Corti lead to oscillations of the hair bundle of the IHCs and OHCs. This mechanosensitive antenna consists of an array of modified microvilli, the stereocilia, which are organized into three rows that are graded in height (i.e., short, middle-sized, and tall stereocilia). The IHC hair bundle is free-standing in the fluid of the subreticular space (i.e., the space between the TM and the organ of Corti), whereas the tips of the tall stereocilia of the OHCs are embedded in the TM. The periodic sound-evoked motion of the TM relative to the surface of the organ of Corti acts as the mechanical stimulus for OHC hair bundles (1). Various types of links connect the stereocilia. In all hair cells, a single fibrous link, the tip link, composed of two cadherin-related proteins, protocadherin 15 and cadherin 23 (2), extends obliquely from the tip of each short and middle-sized stereocilium to the side of the adjacent taller stereocilium. The periodic variation of tip-link tension arising from sound-induced hair bundle oscillation gates the mechano-electrical transduction ion channels, located at the lower insertion point of the tip links, at the tips of short and middle-sized stereocilia (3, 4). OHC stereocilia are also tightly connected to each other by fibrous links attaching their sides (lateral links) (5-8). During development, neighboring stereocilia within and between rows are joined along their shafts by transient lateral links that are no longer present in mature OHCs, and by crown-shaped structures located at the tips of the tall stereocilia. In mature OHCs, these apical structures form the TM-attachment crowns, and the stereocilia are linked laterally, within and between rows, by fibrous links called horizontal top connectors. This name refers to their subapical location between rows and within the tall and middle rows, but they are more broadly distributed within the shortest row of stereocilia. Horizontal top connectors form over a period of a few days, beginning on postnatal day 9 (P9) in mice (7), shortly before the onset of hearing (P12-P13). They have a characteristic zipper-like appearance when viewed by transmission or scanning electron microscopy, due to the presence of a central density. We previously reported that stereocilin, a large secreted protein

defective in the DFNB16 recessive form of prelingual hearing impairment (9), is required for the formation of horizontal top connectors and TM-attachment crowns. In the absence of stereocilin, OHC stereocilia are not connected to each other, and the tall stereocilia are not anchored into the TM, resulting in OHC dysfunction, but with no deleterious effect on IHCs (10, 11). DFNB16 patients suffer from mild-to-moderate hearing impairment that is more pronounced at high than at low sound frequencies (12-17). This auditory phenotype is uncommon among patients with DFNB (nonsyndromic deafness, autosomal recessive) forms of prelingual hearing impairment, who usually suffer from severe or profound deafness as a result of primary defects of both types of hair cells, IHCs alone, or nonsensory (supporting) cells. Notably, audiometric profiles similar to that described for DFNB16 patients have been reported in DFNB18B and DFNB84B patients carrying mutations of *OTOG* (18-20) and *OTOGL* (19, 21-25), respectively. *OTOG* and *OTOGL* encode otogelin and otogelin-like, respectively, two large proteins of the TM related to secreted epithelial mucins (21, 26-28). TM abnormalities can result in abnormal sound-induced stimulation of OHCs, but the unusual auditory phenotype of patients lacking otogelin, otogelin-like, or stereocilin prompted us to explore the possibility that deficiencies of otogelin or otogelin-like could also lead to an intrinsic defect of OHC hair bundles similar to that caused by stereocilin deficiency. We therefore performed morphological and functional analyses of the cochlea of mutant mice lacking otogelin or otogelin-like, and investigated the possible interaction between stereocilin, otogelin, and otogelin-like by studying the distributions of these proteins in the organ of Corti of control and mutant mice.

Results

OHC function is markedly altered in *Otog*^{-/-} mice and *Otogl*^{-/-} mice

The otogelin-deficient mice used in this study, *Otog*^{tm1Prs/tm1Prs} mice (carrying a deletion of the first three exons of *Otog*, referred to hereafter as *Otog*^{-/-} mice), have moderate-to-severe hearing impairment. They also have marked balance disorders due to detachment of the acellular membranes overlying the vestibular sensory epithelia (29). A similar phenotype has been reported in two other mutant lines with otogelin defects, *Otog*^{twl/twl} mice and *Otog*^{vdb/vdb} mice (30, 31). We engineered otogelin-like-deficient mice, *Otogl*^{tm1Ugds/tm1Ugds} mice (referred to hereafter as *Otogl*^{-/-} mice) carrying a frameshift deletion of *Otogl* exons 5 and 6 (see SI Appendix, Materials and methods). Unlike otogelin-deficient mice, these mice displayed no behavioral features of vestibular dysfunction, and had normal results in balance tests (32).

Auditory brainstem responses (ABRs) to bursts of pure tones (5-40 kHz) revealed a substantial threshold difference between mutant mice and their heterozygous controls, stable from P14 to P45 for all frequencies below 32 kHz, reaching 50-60 dB, in both *Otog*^{-/-} mice and *Otogl*^{-/-} mice (Student's *t*-test, $p < 10^{-4}$ for all comparisons with control values, Fig. 1A). However, *Otogl*^{-/-} mice had a slightly lower hearing threshold at 10 kHz than *Otog*^{-/-} mice (mean difference of 4 dB to 11 dB depending on the stage, Student's *t*-test, $p < 0.05$ at P16, P28, and P45). At higher frequencies (32 and 40 kHz), ABR threshold differences between mutants and controls decreased slightly at P28 then P45 likely in relation to a small progressive hearing loss in control mice, inherent to their genetic background. The ABRs to high intensity sounds (> 90 dB SPL) had normal wave amplitudes and latencies in the two mutants, suggesting that IHC function was preserved. Taken together, these results suggest that both mutants display marked isolated OHC dysfunction.

OHCs are also involved in the frequency selectivity of the cochlear response (tuning). We therefore studied this tuning in four-week old *Otog*^{-/-} mice and *Otogl*^{-/-} mice. We established compound action potential (CAP) masking tuning curves, in response to a 10 kHz intermittent probe tone and a continuous masking tone of variable frequency. At low probe intensities, the CAP recorded at the round window reflects the onset responses of the primary afferent neurons from the site in the cochlea tuned to the probe frequency (tonotopic position). The frequency selectivity of sound processing by the cochlea translates into a deep and narrow tip in the masking tuning curve (masking level plotted against masker frequency) around the probe frequency. No frequency tuning was detected in *Otog*^{-/-} mice, whereas some tuning persisted in *Otogl*^{-/-} mice with a measurable $Q_{10\text{dB}}$ (ratio of probe frequency to tuning curve width at 10 dB above its tip: mean value of 2.2 in *Otogl*^{-/-} mice, versus 4.1 in control mice; $p = 0.002$) (Fig. 1B). Cochlear amplification and tuning both arise from the frequency-selective local feedback of electromotile OHCs on cochlear partition. Given that the severity of tuning degradation and the decrease in feedback of electromotile OHCs are correlated (33), the preservation of some tuning in *Otogl*^{-/-} mice and not in *Otog*^{-/-} mice indicates that feedback is slightly less affected in the former mutant.

We then analyzed the cochlear microphonic potential (CM) emitted by the OHCs of the basal coil of the cochlea and recorded at the round window. With a 5 kHz, 90 dB SPL sound stimulus, the CM depends solely on the functionality of the mechano-electrical transduction channels of the basal OHCs, with no requirement for a cochlear amplifier. Shortly after hearing onset (P14-P16), a CM was detected in *Otog*^{-/-} mice and *Otogl*^{-/-} mice, albeit with an amplitude only one third that in *Otog*^{+/-} and *Otogl*^{+/-} control littermates, respectively. Thus, a

substantial proportion of the OHC mechano-electrical transduction channels were functional in both homozygous mutants. However, the CM waveforms were highly asymmetric, suggesting that the operating point of the OHC hair bundles was displaced away from its normal value, at which $\approx 50\%$ of the mechano-electrical transduction channels are open at rest. In addition, the phase of the CM waveform invariably led the CM phase in control heterozygous mice, by 90° in *Otog*^{-/-} mice, and more variably (between 45° and 60°) in *Otogl*^{-/-} mice, consistent with abnormal stimulation of the OHC hair bundles (Fig. 1C).

Given the persistence of functional mechano-electrical transduction channels in OHCs, we expected the use of two-tone stimuli at sufficiently high levels to generate OHC hair bundle displacements of a sizable amplitude even in the absence of cochlear amplification to elicit distortion-product otoacoustic emissions (DPOAEs), as these emissions originate from the nonlinear gating of OHC mechano-electrical transduction channels (see ref. 34 for a review). However, no DPOAEs were detected in *Otog*^{-/-} or *Otogl*^{-/-} mice, regardless of their age, over the 5-20 kHz interval, even for stimuli of > 75 dB SPL (Fig. 1D). For sound stimuli between 22 and 27 kHz, weak DPOAEs emerged from the background noise (which is lowest in this frequency interval), but only for stimuli of > 60 dB SPL, and with maximum amplitudes about 30 dB lower than in control mice (i.e., a 30-fold reduction). The almost total absence of DPOAEs despite the persistence of substantial mechano-electrical transduction currents in the OHCs is reminiscent of observations in young *Strc*^{-/-} mice attributed to the unusual combination of functional mechano-electrical transduction channels within a noncohesive hair bundle (10, 34).

The OHC hair bundles of *Otog*^{-/-} mice and *Otogl*^{-/-} mice lack horizontal top connectors and are not anchored in the TM

We performed scanning electron microscopy studies of the structure of the OHC hair bundles and their connection with the TM in *Otog*^{-/-} and *Otogl*^{-/-} mice. Defects of OHC hair bundle cohesiveness were observed in P14 *Otog*^{-/-} mice and P12-P14 *Otogl*^{-/-} mice (Fig. 2 and SI Appendix, Fig. S1). These defects were associated with an absence (in *Otog*^{-/-} mice), or very small numbers (in *Otogl*^{-/-} mice) of lateral links extending between and within rows of stereocilia, but with some detectable tip links (Fig. 2E). Moreover, no imprints of the tall stereocilia were detected on the lower surface of the TM (Fig. 2 G-I), indicating that the anchoring of the OHC hair bundles in the TM was defective. Both these features have already been reported in *Strc*^{-/-} mice of the same age (10, 11). In addition, the amorphous material covering the tallest row of stereocilia in some wild-type OHCs around P8, indicating close

contact between these stereocilia and the developing TM, was not observed in *Otog*^{-/-} or *Strc*^{-/-} mice (11), but was present in *Otogl*^{-/-} mice (Fig. 2 J-L). These findings suggest that otogelin and stereocilin are involved in early interactions between OHC hair bundles and the TM, whereas otogelin-like is not. Finally, abnormally short stereocilia, or an absence of some stereocilia in the shortest row was frequently observed in the OHCs of *Otog*^{-/-} mice (see Fig. 2K at P9), suggesting a possible defect of stereociliary growth, not observed in *Otogl*^{-/-} mice (examined from P5 to P21) or *Strc*^{-/-} mice.

No OHC loss was observed in two-month-old *Otog*^{-/-} or *Otogl*^{-/-} mice, as in *Strc*^{-/-} mice of the same age (Fig. 3), but the shape of the OHC hair bundles was more severely affected than in the *Strc*^{-/-} mice. The height of stereocilia within a given row was variable, and the typical staircase pattern of the three rows of stereocilia was lost.

Otogelin and otogelin-like are associated with the horizontal top connectors and TM-attachment crowns of the OHC hair bundle

We confirmed previous reports that otogelin and otogelin-like are present in the TM by immunohistofluorescence labeling with new antibodies directed against these proteins (see SI Appendix, Materials and Methods). On P19, otogelin immunostaining of the TM was observed as fiber-like radial strands, thinner on the modiolar side of the TM than on its external side, and dots in the upper part of the TM, along its external edge (Fig. 4A, B, and SI Appendix, Fig. S2). Otogelin-like immunoreactivity also was detected as faint fiber-like radial staining. Additional otogelin-like staining was associated with the three rows of V-shaped imprints characteristic of the anchoring points of the OHC tall stereocilia on the lower surface of the TM, at which the presence of stereocilin had already been reported (11) (Fig. 4D), whereas otogelin staining was not observed at these anchoring points (SI Appendix, Fig. S2). Otogelin and otogelin-like were also detected in the OHC hair bundles of wild-type mice, but the intensity of this immunostaining varied between experiments. We suspected that, as extracellular proteins, otogelin and otogelin-like might be weakly associated with the plasma membrane of the stereocilia, in which case they would be easily lost during the fixation procedure and subsequent removal of the TM. This might also explain the lack of detection of these two proteins in the OHC hair bundles in previous studies. We used *Tecta*^{Δ^{ENT}/Δ^{ENT}} mice (referred to as *Tecta*^{-/-} mice), lacking the TM protein alpha-tectorin, to study the location of otogelin and otogelin-like in OHC hair bundles during postnatal development. In these mice, the TM is constitutively detached from the cochlear epithelium, but the architecture of the organ of Corti is otherwise normal (35). At birth, otogelin was detected around the kinocilium

of both IHCs and OHCs (Fig. 5A). From P1 onward, this protein accumulated at the tips of the tall stereocilia of OHCs (see P6 in Fig. 5B). On P7, it was also detected at the tips of the middle-sized and short stereocilia (Fig. 5C, E). On P15, staining was mostly confined to a subapical position in the middle row, and was more broadly distributed between the stereocilia of the short row, corresponding to the position of the horizontal top connectors (Fig. 5D, F, and Fig. 2D). In the tallest row of stereocilia, staining was restricted to an apical position that was further defined, by immunogold scanning electron microscopy, as surrounding the tips of the stereocilia (Fig. 5E, F), and corresponding to the location of both the TM-attachment crowns and the top connectors (7). This staining pattern was still observed on P21, but, on P30, immunoreactive dots were in much lower number (Fig. 5G, H).

Otogelin-like was first detected on P3, around the kinocilium of both IHCs and OHCs (Fig. 6A). It then progressively accumulated in OHCs, at the tips of the stereocilia of all three rows, initially in the tallest row (see stage P7 on Fig. 6B), and then in the other two rows of stereocilia (see stage P15 in Fig. 6C). On P21, when the organ of Corti is mature, the otogelin-like staining of the middle-sized stereocilia was located in a subapical position consistent with the position of the horizontal top connectors (Fig. 6D). This staining remained unchanged on P30 (Fig. 6E). Otogelin and otogelin-like therefore have similar spatial distributions in the hair bundles of mouse OHCs, but they appear sequentially, with otogelin-like detected a few days after otogelin. Moreover, otogelin-like labeling persisted on P30, whereas otogelin tended to disappear. This spatial expression pattern in the OHC hair bundle is similar to that reported for stereocilin (11). Overall, the lack of horizontal top connectors, TM-attachment crowns, and stereocilia imprints in the TM in *Otog*^{-/-} mice, *Otogl*^{-/-} mice, and *Strc*^{-/-} mice, and the absence of amorphous material (likely derived from the developing TM) covering the tallest stereocilia in the OHCs of young *Otog*^{-/-} mice and *Strc*^{-/-} mice, but not *Otogl*^{-/-} mice 1) indicate that otogelin and otogelin-like are, like stereocilin, components of the horizontal top connectors and TM-attachment crowns of OHC hair bundles, and 2) suggest a developmental scenario in which otogelin and stereocilin are involved in the initial formation of these structures, with otogelin-like contributing to these structures slightly later.

Interdependent distributions of otogelin, otogelin-like, and stereocilin in the cochlea

Given the colocalization of otogelin, otogelin-like, and stereocilin, we investigated the possible interdependence of their distributions. No immunoreactivity for otogelin or otogelin-like was detected in the OHC stereocilia of *Strc*^{-/-} mice and *Strc*^{-/-},*Tecta*^{-/-} mice on P7 and P15 (Fig. 5I, J and 6F, G). Very little immunoreactivity for otogelin or otogelin-like was detected

in the OHCs of P14-P15 *Otogl*^{-/-} mice and *Otog*^{-/-} mice, respectively, and, due to the loss of hair bundle cohesiveness, the scarce signals remaining after the removal of the TM could not be accurately localized. We therefore investigated the interdependence of otogelin and otogelin-like in the TM. In *Otogl*^{-/-} mice, the fiber-like otogelin staining of the TM was much fainter than that in wild-type mice and essentially restricted to thick strands, and the immunoreactive dots observed along the external edge of the TM in control mice were absent (Fig. 4C). In *Otog*^{-/-} mice, both types of otogelin-like staining of the TM (fiber-like and V-shaped hair bundle imprints) were lost (Fig. 4E). The otogelin-like labeling of V-shaped imprints was also lost in *Strc*^{-/-} mice (Fig. 4F).

We also analyzed the distribution of stereocilin in *Otog*^{-/-} mice and *Otogl*^{-/-} mice (Fig. 7). On P6, the immunostaining of the OHC kinocilium in both mutant mice was similar to that in the wild-type mice, but the staining at the tips of the tall stereocilia was lost in *Otog*^{-/-} mice, whereas it was preserved in *Otogl*^{-/-} mice (Fig. 7A-C). Unlike the otogelin and otogelin-like labelings, the stereocilin labeling at the tips of the tall stereocilia of OHCs in P14-P15 or P30 wild-type mice was not significantly affected by the removal of the TM (Fig. 7D, G), suggesting that stereocilin is more tightly associated with the plasma membrane, in keeping with the immunolabeling observed at the surface of transiently transfected HeLa and MDCK cells producing the protein (SI Appendix, Fig. S3). In P14-P17 *Otog*^{-/-} mice and *Otogl*^{-/-} mice, this stereocilin staining was markedly weaker than in wild-type mice. Moreover, its ring-shape distribution was lost, and no stereocilin-immunoreactive V-shaped imprints were observed in the TM (Fig. 7D-L). By contrast, the stereocilin fluorescent labeling of the middle-sized and short stereocilia was strong in both mutants, and staining of middle-sized stereocilia was abnormally located at their tips, instead of being located in a subapical position as in control mice (Fig. 7G-I). Thus, whereas otogelin, otogelin-like, and stereocilin seem to be independently localized around the kinocilium, the absence of any of the three proteins affects the distribution of the other two within the bundle of stereocilia, suggesting that these proteins interact in the hair-bundle links specific to OHCs.

Finally, we studied the distributions of otogelin and otogelin-like in the five mouse models of Usher syndrome type 1 (Ush1). This multisensory disorder, characterized by congenital profound deafness, severe balance disorders, and progressive sight loss, is caused by mutations of the genes encoding myosin VIIa, harmonin, protocadherin 15, cadherin 23, and SANS (scaffold ankyrin and sterile alpha motif containing protein). The hair bundles of the *Myo7a*^{-/-}, *Ush1c*^{-/-}, *Pcdh15*^{-/-}, *Cdh23*^{-/-}, and *Ush1g*^{-/-} (see SI Appendix, Materials and Methods) mutant mice lack tip links and are often fragmented, with a mispositioned kinocilium (36),

probably due to the absence of transient lateral links connecting the stereocilia to each other and to the kinocilium during hair-bundle early development (7, 37, 38). These links are composed of protocadherin 15 and cadherin 23, and their anchoring to the actin core of the stereocilia involves harmonin, SANS, and myosin VIIa (for a review see ref. 39). In the mature OHCs of all these mutants, as well as of the *Pcdh15*^{-/-}, *Cdh23*^{-/-} double-mutant mice (SI Appendix, Fig. S4), we have observed extended stereocilin immunoreactivity associated with an expansion of the contact area between adjacent stereocilia and the presence of additional extracellular matrix at the tips of the stereocilia (10, 11). In mature (P14-P22) OHCs of all *Ush1* mutant mice, otogelin and otogelin-like were observed, like stereocilin, at the tips of stereocilia from different rows. In addition, otogelin (mostly in *Pcdh15*^{-/-} mice) or otogelin-like (noticeably in the four other mutants) immunoreactivity also markedly extended, like stereocilin, between the shafts of adjacent stereocilia (Fig. 8). On P6, a time at which TM-attachment crowns are forming at the tips of the tall stereocilia but the horizontal top connectors have not yet appeared, otogelin and stereocilin were both detected at the tips of all OHC stereocilia in all *Ush1* mutant mice, instead of being restricted to the tips of the tall stereocilia as in wild-type mice (SI Appendix, Fig. S5A), suggesting that TM-attachment crowns may develop at the tips of all OHC stereocilia in these mutants. This is consistent with the presence, in all *Ush1* mouse mutants, of stereocilin and otogelin-like-immunoreactive imprints from unaligned stereocilia in the TM, and of numerous stereocilia torn off from the OHCs and anchored to the TM when removed (SI Appendix, Fig. S5B). We also analyzed the distributions of the three proteins in the OHC hair bundles of *Pcdh15*^{ΔCD2/ΔCD2} mice, which lack only the CD2 isoforms of protocadherin 15. These isoforms form the lower part of the tip links in mature auditory hair cells (40). The distributions of the proteins were not affected on P6, but they were abnormal at mature stages (P15 or P30), with strong immunofluorescent stainings for the three proteins at the tips of the middle-sized and persisting short stereocilia (SI Appendix, Fig. S6A), correlated with an overabundance of lateral links, located in an abnormal, apical position, both within and between rows (SI Appendix, Fig. S6B). Therefore, stereocilin, otogelin, and otogelin-like showed similar abnormal distributions in the absence of any of the *Ush1* protein including the CD2 isoforms of protocadherin 15.

Discussion

Together, our results demonstrate that otogelin and otogelin-like are not only present in the TM, but they also contribute to the horizontal top connectors and TM-attachment crowns of

OHC stereocilia, where they interact, directly or indirectly, with stereocilin. Otogelin and otogelin-like are large secreted proteins (2911 amino acids and 2325 amino acids, respectively, in mice) with 42% identity. Both have a signal peptide, four von Willebrand factor (vWF) domains, four cysteine-rich (C8) domains, an alpha-L arabinofuranosidase B (AbfB) domain, either one (otogelin) or three (otogelin-like) trypsin inhibitor-like (TIL) domains, and a C-terminal cysteine-knot (CTCK) domain. In addition, otogelin-like contains an N-terminal EGF-like domain (Fig. 9A). We have previously shown that otogelin is N-glycosylated but not O-glycosylated, unlike all mucins, and that it can form homodimers but not larger oligomers (26). The presence of a C-terminal CTCK domain in otogelin and otogelin-like indeed suggests that the two proteins likely undergo homodimerization. This domain, which is common to secreted mucins and several other proteins, such as von Willebrand factor and the Norrie disease protein, mediates the antiparallel homodimerization of these proteins in the endoplasmic reticulum (for a minireview see ref. 41). The crystal structure of vWF CTCK dimers has been established. Consistent with previous electron microscopy images of vWF dimers (42), the CTCK dimer has been shown to form a highly force-resistant structure, with 11 pairs of cysteine residues forming disulfide bonds: four within each CTCK monomer, and three across the dimer interface (43). Based on its amino-acid sequence, the CTCK domain of the zebrafish otogelin has been predicted to dimerize in a similar manner (43). All the cysteine residues of the CTCK domain of zebrafish otogelin are conserved in the murine and human otogelin and otogelin-like proteins (Fig. 9B). We therefore suggest that the TM-attachment crowns and horizontal top connectors of OHCs contain dimers of otogelin and dimers of otogelin-like. The dimerized C-terminal CTCK domains of these proteins may form the central density of the horizontal top connectors observed on transmission or scanning electron microscopy images. In agreement with our proposal, electron-dense structures have also been observed at the periphery of the TM-attachment crowns (5-7). The sizes of the densities of the two structures observed on these images are consistent with the 8 nm length of the CTCK dimer derived from electron microscopy images and the crystal structure (43). Stereocilin is a large secreted protein (1809 amino acids in mice) with a large leucine-rich region and several hydrophobic segments, none of which is hydrophobic enough to predict a transmembrane domain (10). Stereocilin, which is tightly associated with the membrane of transfected cells producing it, has been identified as a possible GPI-anchored protein on the basis of a GPI-modification site predicted by the DGPI algorithm (by Kronegg J and Buloz D, retrieved 20070709 from <http://129.194.185.165/dgpi/>) in the mouse sequence (44). However, using the same algorithm

or PredGPI (45), we found a predicted GPI-anchor in the stereocilin sequence of some (e.g., mouse) but not other (e.g., human) species, and big-PI prediction (46) did not identify a potential GPI-modification site in any species. Thus, the way in which stereocilin associates with the plasma membrane remains to be determined. Given the absence of otogelin and otogelin-like detection in OHC hair bundles in the absence of stereocilin, we suggest that the otogelin and otogelin-like antiparallel dimers are associated with the membrane of the stereocilia through stereocilin (see Fig. 9C for a model). When the TM-attachment crowns form at the tips of the OHC tall stereocilia, stereocilin and otogelin require each other for their localization at this position, whereas the distribution of stereocilin is not dependent on the presence of otogelin-like. However, in mature OHCs, otogelin-like is required for the connection of the tall stereocilia to the TM, and otogelin, although still present at the tips of the tall stereocilia, is not detected at the interface between these stereocilia and the TM lower surface. Otogelin and, shortly after, otogelin-like are first targeted to the tips of the middle-sized and short stereocilia, and then to subapical positions, at the site of the horizontal top connectors, where otogelin-like ultimately becomes largely predominant in mature OHCs (Fig. 5H, 6E). We suggest that the first horizontal top connectors formed contain otogelin and stereocilin, and that these connectors are subsequently replaced by connectors containing otogelin-like and stereocilin (Fig. 9C). As a corollary, otogelin and otogelin-like may form different subtypes of connectors containing antiparallel homodimers of either protein. In addition, the use of either otogelin or otogelin-like, and of their various protein isoforms, as already reported for otogelin (26), may provide a means of adapting the size of the connectors to the space between adjacent stereocilia within and between rows. This molecular diversity may also open up possibilities for accommodating putative tonotopic variations of the mechanical properties of these links.

Some audiometric features are common to *Strc*^{-/-}, *Otog*^{-/-}, and *Otogl*^{-/-} mice, whereas others are common only to *Otog*^{-/-} and *Otogl*^{-/-} mice. The features common to the three mutants are probably accounted for by defects of the OHC horizontal top connectors and TM-attachment crowns, both of which contain all three proteins, whereas the features common only to *Otog*^{-/-} and *Otogl*^{-/-} mice are probably related to defects of the TM, which contains otogelin and otogelin-like, but not stereocilin. The striking finding of an absence of acoustic distortion products, even for high-level sound stimuli, despite the persistence of mechano-electrical transduction in the OHCs, first reported in young *Strc*^{-/-} mice, extends to *Otog*^{-/-} mice and *Otogl*^{-/-} mice. Unlike these three mutants, *Tecta*^{ΔENT/ΔENT} mice display DPOAEs in response to tone pairs above 65 dB SPL, rapidly increasing with the intensity of the stimulus to reach

values within 10 dB of normal DPOAEs (47). The finding that *Otog*^{-/-} and *Otogl*^{-/-} mice, like *Strc*^{-/-} mice, lack OHC horizontal top connectors and TM-attachment crowns, whereas *Tecta*^{ΔENT/ΔENT} mice only have absent OHC-TM coupling, confirms that the top connectors, which ensure OHC hair bundle cohesiveness, play a crucial role in the generation of sizeable DPOAEs in the ear canal (10). The tips of the tall stereocilia of the OHCs are not embedded in the TM in any of these mutants. However, the functional impact on the phase of the CM potentials, which reflects the timing of mechano-electrical transduction channel gating in basal OHCs, differs between these mutants. The phase of the CM was not shifted in *Strc*^{-/-} mice (10), but showed a variable lead in *Otogl*^{-/-} mice, increasing to 90° in *Otog*^{-/-} mice with respect to that in heterozygous control mice. The phase relationship between the mechanical contraction/elongation response of OHCs to sound (electromotility), driven by the oscillation of their membrane potential (from which the CM potential arises), and the stimulus-driven motion of the TM is thought to be critical for the correct timing of mechanical feedback of OHC electromotility on the motion of the organ of Corti (48, 49). A phase shift in the oscillation of OHC membrane potential would therefore be expected to compromise subsequent steps towards amplification. Starting from a 60-dB amplification and a normal CM phase, the cochlear-amplifier gain would be expected to decline with shifts in CM phase. Our observations are consistent with this prediction, with amplification and tuning initially preserved in young *Strc*^{-/-} mice with a normal CM phase (10), whereas hearing thresholds at 10 kHz are a mean of 60 dB higher in *Otog*^{-/-} mice, which display a 90°-CM phase shift, and 53 dB higher in *Otogl*^{-/-} mice, which have an intermediate phase shift. Likewise, tuning at 10 kHz is virtually absent in *Otog*^{-/-} mice, whereas it is weak but still present in *Otogl*^{-/-} mice. The CM phase shift in *Otog*^{-/-} mice is similar to that for *Tecta*^{ΔENT/ΔENT} mice with defects of alpha-tectorin, in which the abnormal TM is completely detached from the sensory epithelium, thus losing its ability to drive OHC hair bundle oscillations (35). Given that the TM is not detached in *Otog*^{-/-} mice and *Otogl*^{-/-} mice, we suggest that the shifted CM phase in these two mutants probably results from abnormal functional coupling between the TM and OHC hair bundles, with variable contribution of abnormalities in the mechanical properties of the TM (expected to be more pronounced in *Otog*^{-/-} mutants than in *Otogl*^{-/-} mutants). Another feature common to *Otog*^{-/-} and *Otogl*^{-/-} mice, already reported in *Tecta*^{ΔENT/ΔENT} mice, but absent in young *Strc*^{-/-} mice, is the CM asymmetric profile (35). It indicates that the presence of a TM overlying the sensory epithelium (as observed in *Otog*^{-/-} mice, *Otogl*^{-/-} mice, and *Strc*^{-/-} mice) is a necessary, but not sufficient condition for proper control of the OHC-hair-bundle

operating point by the TM (47), and that the presence of otogelin and otogelin-like in the TM is required for this control.

The site-specific analysis of sound wave frequency components in the mammalian cochlea (tonotopy) involves local amplification of the passive motion of the organ of Corti by a group of tuned OHCs, which operate collectively in a phase-coherent manner relative to the vibration of the underlying basilar membrane. This involves different levels of local mechanical coupling. Firstly, the cooperation of neighboring OHCs depends on the intricate arrangement of these cells with the apical processes of the Deiters' and outer pillar supporting cells, which form tight junctions with the apico-lateral walls of OHCs (50, 51), thereby forming a stiff mosaic (reticular lamina) at the surface of the epithelium. The phase differences between the displacements of the reticular lamina and the basilar membrane are tightly constrained (52). In addition, the anchoring of the tall stereocilia of the OHCs in the TM probably results in a local elastic connection between the hair bundles of neighboring OHCs, which, by reducing the intrinsic noise of these oscillatory elements, would enhance mechanical amplification (53). Finally, at a subcellular level, the horizontal top connectors, by holding OHC stereocilia tightly together, probably ensure that the hair bundle moves as a single unit, triggering parallel gating of the mechano-electrical transduction channels, as shown in the hair cells of the bullfrog saccule (34, 54). This previous study also led to generic models of sliding adhesion, in which sliding could occur between stereocilia despite the stiff lateral links holding them together (54). The predicted interactions between stereocilin and otogelin or otogelin-like dimers, and between stereocilin and the plasma membrane provide a substratum for the evaluation of these models. In this context, the molecular kinship of the horizontal top connectors and TM-attachment crowns shown here is quite remarkable, and raises the possibility that these two structures also have shared mechanical features relating to their critical roles in the stimulation of the OHC hair bundles.

Materials and methods

A detailed description is available in the SI Appendix, including a description of the animals, auditory tests, antibodies, immunostaining, scanning electron microscopy procedures, and cell transfection experiments. Animal experiments were performed in accordance with the French and European regulations for the protection of animals used for scientific purposes (project authorization number 00274.03) with approval from the Animal Ethics Committee of the Pasteur Institute (CETEA-Institut Pasteur, project number 2013-0057).

Data Availability

The data and materials that support the findings of this study are available from the corresponding authors upon reasonable request.

Acknowledgments

We thank Jacques Boutet de Monvel for helpful comments on the manuscript, and Jérémie Chatel-Poujade, Isabelle Perfettini, and Céline Trébeau for technical assistance. This work was supported by the European Commission (ERC-2011-ADG-294570 to C.P.), BNP Paribas, Fondation pour l'Audition, LHW-Stiftung, and by French state funds managed by the ANR within the "Investissement d'Avenir" program (ANR-15-RHUS-0001 and LabEx Lifesenses ANR-10-LABX-65) and ANR-16-CE13-0015-02.

References

1. Ashmore J (2008) Cochlear outer hair cell motility. *Physiological Reviews* 88(1):173-210.
2. Kazmierczak P, *et al.* (2007) Cadherin 23 and protocadherin 15 interact to form tip-link filaments in sensory hair cells. *Nature* 449(7158):87-91.
3. Markin VS & Hudspeth AJ (1995) Gating-spring models of mechano-electrical transduction by hair-cells of the internal ear. *Annu Rev Biophys Biom* 24:59-83.
4. Beurg M, Fettiplace R, Nam JH, & Ricci AJ (2009) Localization of inner hair cell mechanotransducer channels using high-speed calcium imaging. *Nat Neurosci* 12(5):553-558.
5. Tsuprun V & Santi P (1998) Structure of outer hair cell stereocilia links in the chinchilla. *J Neurocytol* 27(7):517-528.
6. Tsuprun V & Santi P (2002) Structure of outer hair cell stereocilia side and attachment links in the chinchilla cochlea. *J Histochem Cytochem* 50(4):493-502.
7. Goodyear RJ, Marcotti W, Kros CJ, & Richardson GP (2005) Development and properties of stereociliary link types in hair cells of the mouse cochlea. *J Comp Neurol* 485(1):75-85.
8. Furness DN & Hackney CM (2006) The structure and composition of the stereociliary bundle of vertebrate hair cells. *Vertebrate hair cells*, eds Eatock R & R. FR (Springer-Verlag, New York), pp 95-153.
9. Verpy E, *et al.* (2001) Mutations in a new gene encoding a protein of the hair bundle cause non-syndromic deafness at the DFNB16 locus. *Nat Genet* 29(3):345-349.
10. Verpy E, *et al.* (2008) Stereocilin-deficient mice reveal the origin of cochlear waveform distortions. *Nature* 456(7219):255-258.
11. Verpy E, *et al.* (2011) Stereocilin connects outer hair cell stereocilia to one another and to the tectorial membrane. *J Comp Neurol* 519(2):194-210.
12. Campbell DA, *et al.* (1997) A new locus for non-syndromal, autosomal recessive, sensorineural hearing loss (DFNB16) maps to human chromosome 15q21-q22. *J Med Genet* 34(12):1015-1017.
13. Villamar M, del Castillo I, Valle N, Romero L, & Moreno F (1999) Deafness locus DFNB16 is located on chromosome 15q13-q21 within a 5-cM interval flanked by markers D15S994 and D15S132. *Am J Hum Genet* 64(4):1238-1241.
14. Francey LJ, *et al.* (2012) Genome-wide SNP genotyping identifies the Stereocilin (*STRC*) gene as a major contributor to pediatric bilateral sensorineural hearing impairment. *Am J Med Genet A* 158A(2):298-308.
15. Mandelker D, *et al.* (2014) Comprehensive diagnostic testing for stereocilin: an approach for analyzing medically important genes with high homology. *J Mol Diagn* 16(6):639-647.
16. Vona B, *et al.* (2015) DFNB16 is a frequent cause of congenital hearing impairment: implementation of *STRC* mutation analysis in routine diagnostics. *Clin Genet* 87(1):49-55.
17. Yokota Y, *et al.* (2019) Frequency and clinical features of hearing loss caused by *STRC* deletions. *Sci Rep* 9(1):4408.
18. Schraders M, *et al.* (2012) Mutations of the gene encoding otogelin are a cause of autosomal-recessive nonsyndromic moderate hearing impairment. *Am J Hum Genet* 91(5):883-889.
19. Oonk AM, *et al.* (2014) Similar phenotypes caused by mutations in *OTOG* and *OTOGL*. *Ear Hear* 35(3):e84-91.
20. Yu S, *et al.* (2019) A novel early truncation mutation in *OTOG* causes prelingual mild hearing loss without vestibular dysfunction. *Eur J Med Genet* 62(1):81-84.

21. Yariz KO, *et al.* (2012) Mutations in *OTOGL*, encoding the inner ear protein otogelin-like, cause moderate sensorineural hearing loss. *Am J Hum Genet* 91(5):872-882.
22. Bonnet C, *et al.* (2013) Biallelic nonsense mutations in the otogelin-like gene (*OTOGL*) in a child affected by mild to moderate hearing impairment. *Gene* 527(2):537-540.
23. Gu X, *et al.* (2015) Novel biallelic *OTOGL* mutations in a Chinese family with moderate non-syndromic sensorineural hearing loss. *Int J Pediatr Otorhinolaryngol* 79(6):817-820.
24. Kim NK, *et al.* (2015) Whole-exome sequencing reveals diverse modes of inheritance in sporadic mild to moderate sensorineural hearing loss in a pediatric population. *Genet Med* 17(11):901-911.
25. Barake R, Abou-Rizk S, Nemer G, & Bassim M (2017) The *OTOGL* p.Arg925* variant is associated with moderate hearing loss in a syrian nonconsanguineous family. *Genet Test Mol Biomarkers* 21(7):445-449.
26. Cohen-Salmon M, El-Amraoui A, Leibovici M, & Petit C (1997) Otogelin: a glycoprotein specific to the acellular membranes of the inner ear. *Proc Natl Acad Sci USA* 94(26):14450-14455.
27. El-Amraoui A, Cohen-Salmon M, Petit C, & Simmler MC (2001) Spatiotemporal expression of otogelin in the developing and adult mouse inner ear. *Hear Res* 158(1-2):151-159.
28. Shahin H, *et al.* (2010) Nonsense mutation of the stereociliar membrane protein gene *PTPRQ* in human hearing loss DFNB84. *J Med Genet* 47(9):643-645.
29. Simmler MC, *et al.* (2000) Targeted disruption of otog results in deafness and severe imbalance. *Nat Genet* 24(2):139-143.
30. Simmler MC, *et al.* (2000) Twister mutant mice are defective for otogelin, a component specific to inner ear acellular membranes. *Mamm Genome* 11(11):960-966.
31. El Hakam Kamareddin C, Magnol L, & Blanquet V (2015) A new Otogelin ENU mouse model for autosomal-recessive nonsyndromic moderate hearing impairment. *Springerplus* 4:730.
32. Steel KP & Hardisty R (1996) Assessing hearing, vision and balance in mice. *What's wrong with my mouse? New interplays between mouse genes and behavior*, eds Society for Neuroscience - Short Course Syllabus (Washington DC), pp 26-38.
33. Davis H (1983) An active process in cochlear mechanics. *Hear Res* 9(1):79-90.
34. Avan P, Buki B, & Petit C (2013) Auditory distortions: origins and functions. *Physiol Rev* 93(4):1563-1619.
35. Legan PK, *et al.* (2000) A targeted deletion in alpha-tectorin reveals that the tectorial membrane is required for the gain and timing of cochlear feedback. *Neuron* 28(1):273-285.
36. Lefevre G, *et al.* (2008) A core cochlear phenotype in USH1 mouse mutants implicates fibrous links of the hair bundle in its cohesion, orientation and differential growth. *Development* 135(8):1427-1437.
37. Petit C & Richardson GP (2009) Linking genes underlying deafness to hair-bundle development and function. *Nat Neurosci* 12(6):703-710.
38. Goodyear RJ, Forge A, Legan PK, & Richardson GP (2010) Asymmetric distribution of cadherin 23 and protocadherin 15 in the kinocilial links of avian sensory hair cells. *J Comp Neurol* 518(21):4288-4297.
39. El-Amraoui A & Petit C (2005) Usher I syndrome: unravelling the mechanisms that underlie the cohesion of the growing hair bundle in inner ear sensory cells. *J Cell Sci* 118(Pt 20):4593-4603.
40. Pepermans E, *et al.* (2014) The CD2 isoform of protocadherin-15 is an essential component of the tip-link complex in mature auditory hair cells. *EMBO Mol Med* 6(7):984-992.

41. Perez-Vilar J & Hill RL (1999) The structure and assembly of secreted mucins. *J Biol Chem* 274(45):31751-31754.
42. Zhou YF, *et al.* (2011) A pH-regulated dimeric bouquet in the structure of von Willebrand factor. *EMBO J* 30(19):4098-4111.
43. Zhou YF & Springer TA (2014) Highly reinforced structure of a C-terminal dimerization domain in von Willebrand factor. *Blood* 123(12):1785-1793.
44. Jovine L, Park J, & Wassarman PM (2002) Sequence similarity between stereocilin and otoancorin points to a unified mechanism for mechanotransduction in the mammalian inner ear. *BMC Cell Biol* 3:28.
45. Pierleoni A, Martelli PL, & Casadio R (2008) PredGPI: a GPI-anchor predictor. *BMC Bioinformatics* 9:392.
46. Eisenhaber B, Bork P, & Eisenhaber F (1999) Prediction of potential GPI-modification sites in proprotein sequences. *J Mol Biol* 292(3):741-758.
47. Lukashkin AN, Lukashkina VA, Legan PK, Richardson GP, & Russell IJ (2004) Role of the tectorial membrane revealed by otoacoustic emissions recorded from wild-type and transgenic *Tecta*^{ΔENT/ΔENT} mice. *J Neurophysiol* 91(1):163-171.
48. Gummer AW, Hemmert W, & Zenner HP (1996) Resonant tectorial membrane motion in the inner ear: its crucial role in frequency tuning. *Proc Natl Acad Sci USA* 93(16):8727-8732.
49. Lukashkin AN, Richardson GP, & Russell IJ (2010) Multiple roles for the tectorial membrane in the active cochlea. *Hear Res* 266(1-2):26-35.
50. Soons JA, Ricci AJ, Steele CR, & Puria S (2015) Cytoarchitecture of the mouse organ of corti from base to apex, determined using in situ two-photon imaging. *J Assoc Res Otolaryngol* 16(1):47-66.
51. Motallebzadeh H, Soons JAM, & Puria S (2018) Cochlear amplification and tuning depend on the cellular arrangement within the organ of Corti. *Proc Natl Acad Sci USA* 115(22):5762-5767.
52. Ren TY, He WX, & Kemp D (2016) Reticular lamina and basilar membrane vibrations in living mouse cochleae. *Proc Natl Acad Sci USA* 113(35):9910-9915.
53. Barral J, Dierkes K, Lindner B, Julicher F, & Martin P (2010) Coupling a sensory hair-cell bundle to cyber clones enhances nonlinear amplification. *Proc Natl Acad Sci USA* 107(23):10765-10765.
54. Karavitaki KD & Corey DP (2010) Sliding adhesion confers coherent motion to hair cell stereocilia and parallel gating to transduction channels. *J Neurosci* 30(27):9051-9063.

Figures

Figure 1. Auditory tests in *Otog*^{-/-} and *Otogl*^{-/-} mice

Results for *Otog*^{-/-} (diagrams on the left) and *Otogl*^{-/-} (diagrams on the right) mutant mice, and for aged-matched *Otog*^{+/-} and *Otogl*^{+/-} controls are presented in blue and in red/brown, respectively (different shades of blue and red/brown for different ages). The numbers of animals studied for each genotype are indicated in brackets. (A) Auditory brainstem response (ABR) thresholds (mean \pm SD) in response to short tone pips at different frequencies (horizontal axis) and at different ages. (B) Masking tuning curves in P28 mice (mean \pm SD) showing the intensity level against frequency of a continuous tone (masker) required for a 50% decrease in amplitude of the compound action potential produced by a 10-kHz tone pip (test tone) presented at 10 dB above the ABR threshold. (C) Steady-state cochlear microphonic potential (CM) recorded in P16 mice with an electrode located at the round window, and produced by a long, 5-kHz tone pip at 95 dB SPL. Note the asymmetry and phase shifts of the waveforms in the mutant mice relative to the control mice. (D) Distortion product otoacoustic emission (DPOAE) thresholds (mean \pm SD) for two-tone stimuli (frequencies f_1 and f_2 , at equal intensities) across the f_2 frequency in P16 mice. Vertical arrows indicate the absence of DPOAE for the maximal intensity of the stimulus (75 dB SPL).

Figure 2. Scanning electron micrographs of the OHC hair bundles and TM in wild-type, *Otog*^{-/-}, and *Otogl*^{-/-} mice at and before the onset of hearing

D, E and F are enlargements of the regions boxed in A, B, and C, respectively. (A, D) In mouse OHCs, there is no clear boundary between the TM-attachment crowns and the horizontal top connectors of tall stereocilia (arrow in D). In addition, the so-called horizontal top connectors between short stereocilia are broadly distributed along their shafts (arrowheads in D). Horizontal top connectors between adjacent stereocilia belonging to different rows are indicated by double arrowheads in D. In P14 *Otog*^{-/-} mice (B, E), the OHC hair bundles display a lack of cohesiveness, due to the absence of apical crowns on the tall stereocilia and horizontal top connectors between and within rows, whereas some tip links are still detected (arrows in E). In P12 *Otogl*^{-/-} mice (C, F), only sparse links (arrows) are observed between the stereocilia. In P14 wild-type mice (G), but not *Otog*^{-/-} (H) or *Otogl*^{-/-} (I) mice, three rows of V-shaped imprints (arrows in G) left by the anchoring of the OHC tall stereocilia in the TM can be seen on the lower surface of the TM. Arrowheads in G-I point to the external edge of the TM, and curved black arrows in H and I indicate that the external margin of the TM is lifted

up. On P7-P9, an amorphous material is observed covering (partially or completely) the tallest row of stereocilia of some OHCs in wild-type and *Otogl*^{-/-} mice (arrows in J and L), but not in *Otog*^{-/-} mice (K). In *Otog*^{-/-} OHCs, the stereocilia of the short row may be abnormally short or even missing (K), but this defect is variable, with almost all stereocilia of the short row being of normal size in some OHCs (B and * in K) and an almost complete absence of normal-sized stereocilia in others (** in K). Scale bars: 1 μm (A-C), 0.3 μm (D-F), 5 μm (G-I), or 2 μm (J-L).

Figure 3. Scanning electron micrographs of OHC hair bundles in adult wild-type, *Otog*^{-/-}, *Otogl*^{-/-}, and *Strc*^{-/-} mice

In addition to the absence of lateral links between stereocilia already evident at hearing onset, the OHC hair bundles of P60 *Otog*^{-/-} mice (C, D) and *Otogl*^{-/-} mice (E, F) display modified staircase patterns, with the stereocilia differing in height within rows. This defect shows marked variability between OHCs (C, E), and was not detected in the OHCs of *Strc*^{-/-} mice (G, H). Scale bars: 4 μm (A, C, E, G) or 2 μm (B, D, F, H).

Figure 4. Otogelin and otogelin-like in the TM

Full z-compressions of confocal images of the entire thickness of TM whole-mount preparations immunostained for otogelin (A-C) or for otogelin-like (D-F) in P19-P25 wild-type, *Otogl*^{-/-}, *Otog*^{-/-}, and *Strc*^{-/-} mice. B is a detailed view of the external part of the TM. The dashed lines in E indicate TM edges. Scale bars: 40 μm (A, C-F), or 10 μm (B).

Figure 5. Otogelin in the developing and mature OHCs

Confocal images of whole-mount preparations of the organ of Corti immunostained for otogelin (green), and stained for actin (red), in *Tecta*^{-/-} mice (A-D, G, H) and *Strc*^{-/-}, *Tecta*^{-/-} double mutant mice (I-J), and scanning electron micrographs of OHC hair bundles after otogelin immunolabeling in *Tecta*^{-/-} mice (E, F). Double arrowheads (A, B, E) indicate the transient kinocilium in P0-P7 inner hair cells (IHC) and OHCs (three rows denoted OHC1, OHC2, and OHC3), which has disappeared on P15. Arrows (C, D) indicate the immunostaining in the distal region of middle-sized stereocilia, just above their tip on P7 (C), and in a subapical location corresponding to the position of horizontal top connectors on P15 (D). Immunostained dots are much fewer on P30 (H) than on P15 (D) and P21 (G), and are not seen in the absence of stereocilin (I, J). Scale bars: 5 μm (A-D, G-J) or 0.5 μm (E, F).

Figure 6. Otogelin-like in the developing and mature OHCs

Confocal images of whole-mount preparations of the organ of Corti immunostained for otogelin-like (green), and stained for actin (red), in *Tecta*^{-/-} mice and *Strc*^{-/-},*Tecta*^{-/-} double mutant mice. Double arrowheads (A, B) indicate the transient kinocilium in immature inner hair cells (IHCs) and OHCs (three rows denoted OHC1, OHC2, and OHC3). Arrows (C, D) indicate the immunostaining in the distal region of middle-sized stereocilia, just above the tip on P15 (C), and in a subapical location corresponding to the position of the horizontal top connectors on P21 (D). Otogelin-like immunostaining persists on P30 (E), and is not seen in the absence of stereocilin (F, G). Scale bars: 5 μm.

Figure 7. Stereocilin in the OHCs and TM of wild-type, *Otog*^{-/-}, and *Otogl*^{-/-} mice before and after the onset of hearing

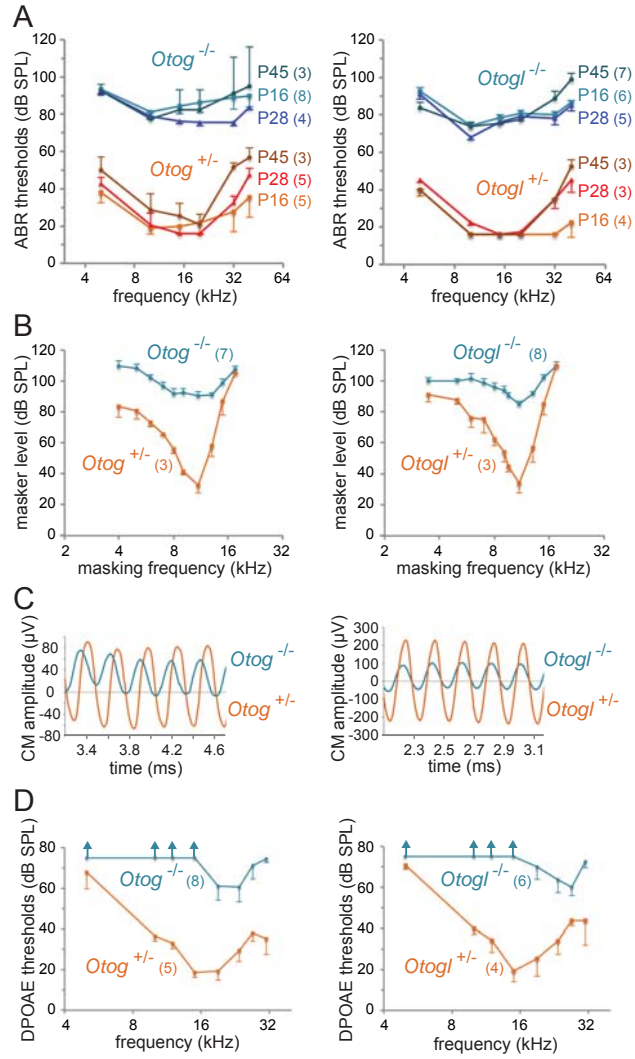
Confocal images (A-C, G-L) and scanning electron micrographs (D-F) of the OHC hair bundles (A-I) and TM (J-L) immunolabeled for stereocilin (gold particles on scanning electron micrographs, and green staining on confocal images), and stained for actin (red) on confocal images. Double arrowheads in (A-C) indicate the transient kinocilium still present in some hair cells on P6. In the P14 wild-type mouse, but not in *Otog*^{-/-} or *Otogl*^{-/-} mice of the same age, three parallel rows of stereocilin-immunoreactive V-shaped imprints are observed at the anchoring points of the OHC tall stereocilia, on the external side of the TM lower surface (J-L; the dashed lines indicate the edges of the TM in mutant mice). Scale bars: 5 μm (A-C, G-I), 0.5 μm (D-F), or 50 μm (J-L).

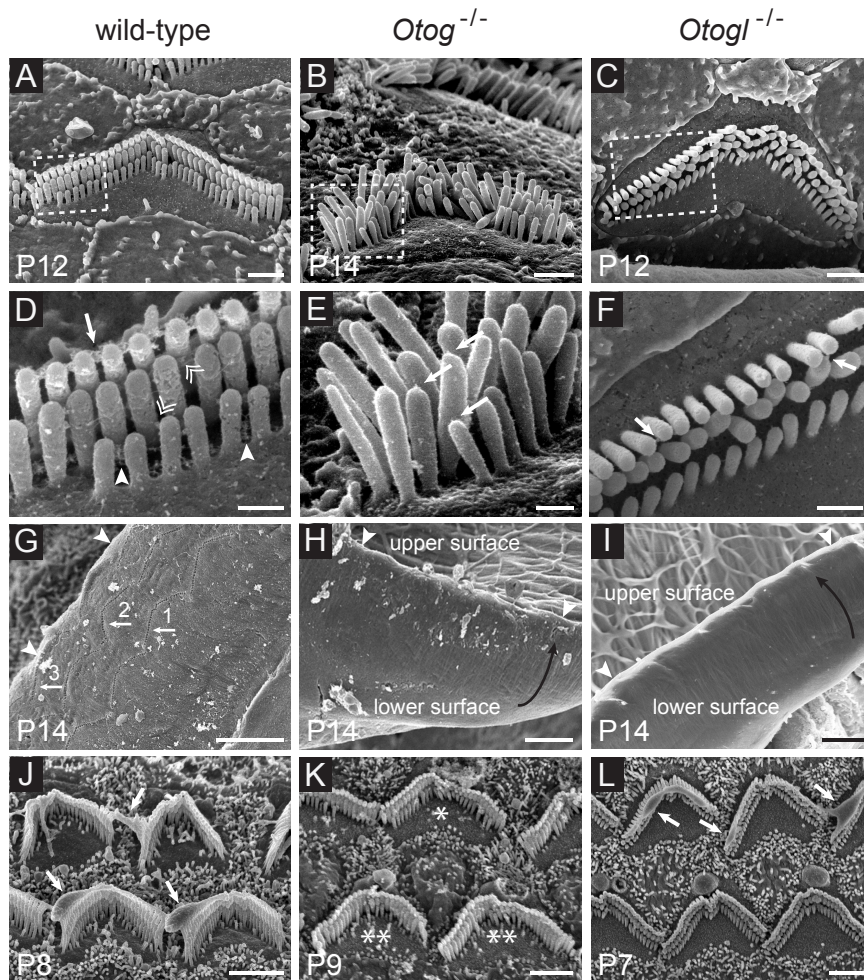
Figure 8. Otogelin and otogelin-like in mouse models of the five different genetic forms of Usher syndrome type 1

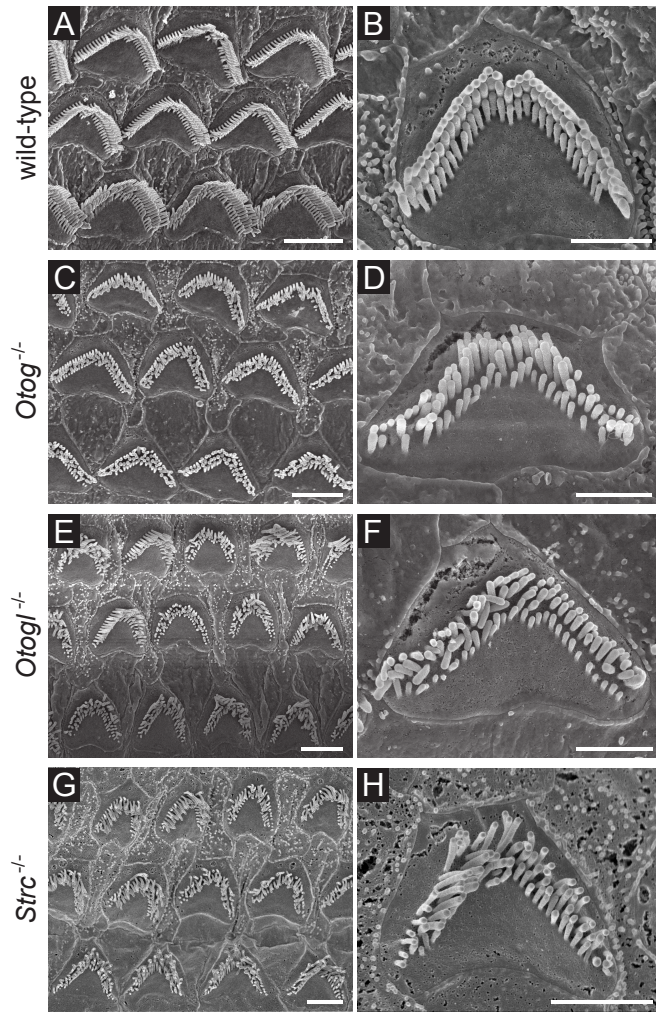
Confocal images of OHCs immunostained for either otogelin (left panels) or otogelin-like (right panels) (in green or white), and stained for actin (red). In *Pcdh15*^{-/-} mice, otogelin is detected both at the tips of the stereocilia and between stereocilia, and otogelin-like is detected mostly at the tips of the stereocilia. In the other four mutants, otogelin is located mostly at the tips of the stereocilia, whereas otogelin-like is detected both at the tips and between stereocilia. Scale bars: 5 μm.

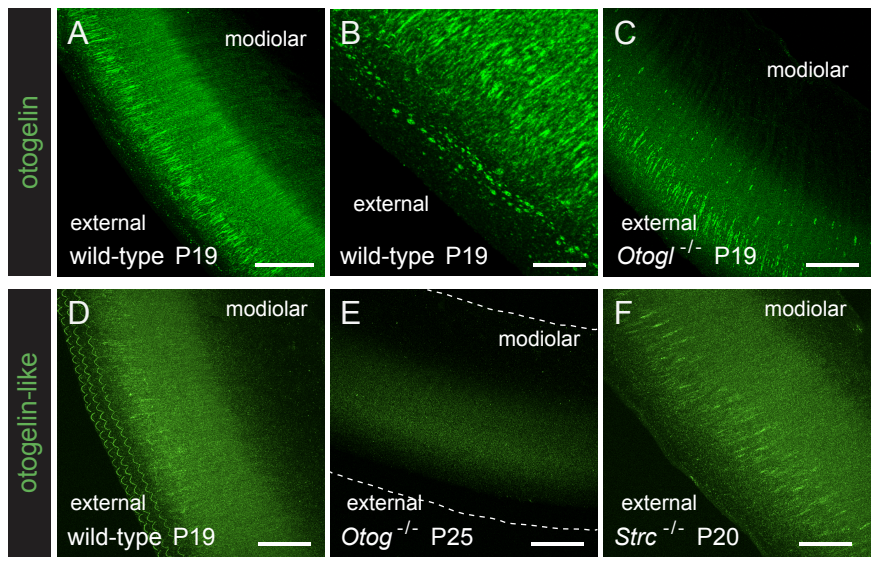
Figure 9. Otogelin and otogelin-like in the formation of TM-attachment crowns and horizontal top connectors in OHC hair bundles

(A) Modular structure of the mouse otogelin and otogelin-like proteins. SP, signal peptide; EGF-like, epidermal growth factor-like domain; VWD, von Willebrand factor-like domain; C8, cysteine-rich domain; TIL, trypsin inhibitor-like domain; AbfB, alpha-l-arabinofuranosidase B-like domain; CTCK, C-terminal cystine knot domain. (B) Comparison of the amino-acid sequences of CTCK domains in the human (*Homo sapiens*, *Hs*) von Willebrand factor (VWF) and in the zebrafish (*Danio rerio*, *Dr*), mouse (*Mus musculus*, *Mm*), and human (*Hs*) otogelin (OTOG) and otogelin-like (OTOGL) proteins. According to the crystal structure of the VWF CTCK dimer (43), the three cysteine residues forming interchain disulfide bonds are highlighted in gray, and the four cysteine pairs forming disulfide bonds within each CTCK monomer are highlighted in yellow, blue, green, and orange. Amino-acid residues conserved in the OTOG and OTOGL sequences of *Dr*, *Mm*, and *Hs* are highlighted in purple. (C) Proposed model for the formation of TM-attachment crowns and horizontal top connectors in immature and mature mouse OHCs. The model is based on the antiparallel homodimerization of otogelin and otogelin-like in the endoplasmic reticulum through the C-terminal cysteine knot domain, and the close association of stereocilin with the plasma membrane. The interaction between stereocilin and otogelin or otogelin-like may be direct or indirect. The postnatal formation of the immature crowns initially involves stereocilin and otogelin, with the incorporation of otogelin-like at later stages. The first horizontal top connectors between the middle-sized stereocilia contain otogelin dimers bound to stereocilin. A few days later, new connectors contain otogelin-like dimers and stereocilin.

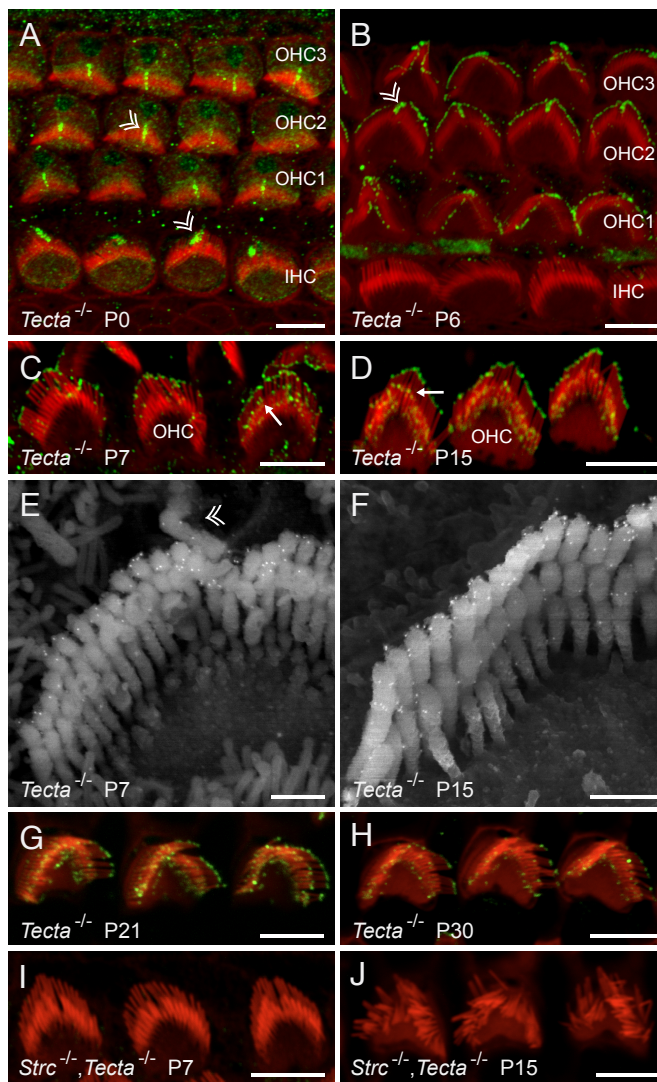








otogelin



otogelin-like

